

Received 16 August 2025, accepted 28 August 2025, date of publication 3 October 2025, date of current version 13 October 2025.

Digital Object Identifier 10.1109/ACCESS.2025.3617323



RESEARCH ARTICLE

Generating Measurement-Based Synthetic Received Signal Power Data for 6G Sub-Terahertz Research With Micromobility and Blockage

VITALII BESCHASTNYI[©]1,², MARGARITA ERSHOVA[©]1,³, DARYA OSTRIKOVA[©]2, VLADISLAV PROSVIROV[©]1, ALEXANDER SHURAKOV[©]1,³, YULIYA GAIDAMAKA[©]2, YEVGENI KOUCHERYAVY[©]1, AND GREGORY GOL'TSMAN[©]1,^{3,4}

¹Telecommunications Research and Development Institute, MIEM, HSE University, 101000 Moscow, Russia

Corresponding author: Vitalii Beschastnyi (vbeschastnyi@hse.ru)

Support from the Basic Research Program of HSE University is gratefully acknowledged.

ABSTRACT Blockage of propagation paths between the base station (BS) and user equipment (UE), as well as the micromobility of the UE, are known to be critical phenomena affecting the performance of 6G subterahertz/terahertz (sub-THz/THz, 0.1–0.3/0.3–3 THz) cellular systems. The development of functions that target the performance improvement of such systems requires understanding of the dynamics of the received signal. However, measurements of the signal received power (SRP) reported to date are limited to the blockage and micromobility phenomena in isolation. In this study, by utilizing individual measurements of blockage and micromobility processes, we propose a procedure for generating synthetic time series of the received signal strength simultaneously capturing blockage, micromobility, and beam-tracking procedures. Our results reveal that out of all the considered applications, only the most dynamic ones, racing game and VR, are characterized by significant differences between on-demand and regular beam tracking with 4-6.5 bits/Hz/s spectral efficiency degradation in the case of on-demand beam tracking as compared to the regular one. For applications with high-speed micromobility (VR watching and race gaming), the minimal beam tracking interval is 80 ms, whereas for low-speed applications, a period of 320 ms and even sometimes 1000 ms is sufficient. Our results show that the availability of information regarding the type of application allows one to decrease the overhead required for beam tracking by up to 20-30 times. The traces produced can be further utilized for various tasks, including the development of statistical tests for discriminating blockage and micromobility events, designing blockage detection algorithms, and improving beam tracking procedures. We made the data produced available to the research community

INDEX TERMS 6G, subterahertz, signal received power, measurements, blockage, micromobility, outage, beam tracking.

I. INTRODUCTION

Sixth-generation (6G) and future cellular communications systems are expected to occupy the subterahertz band (sub-THz, 100–300 GHz) first, and then go even further to truly terahertz (THz, 0.3–3 THz) frequencies, providing

The associate editor coordinating the review of this manuscript and approving it for publication was Barbara Masini^D.

an enormous bandwidth at the air interface. Although the development of these systems has already been initiated within 3GPP by forming a special interest group [1], the accumulated knowledge about propagation effects and impairments is still fragmented.

Several phenomena affect the performance of sub-THz/THz channels. Among these, the blockage of propagation paths between the base station (BS) and user equipment

²Peoples' Friendship University of Russia (RUDN University), 117198 Moscow, Russia

³Moscow Pedagogical State University, 119435 Moscow, Russia

⁴Russian Quantum Center, 143026 Skolkovo Innovation Center, Russia



(UE) by human bodies [2], [3], and the micromobility of UEs in the user's hands are unique to high-frequency bands utilized in 5G/6G systems. The latter occurs even when the user is in a stationary position, depends heavily on the type of utilized application, and is mainly caused by rotations of the UE over the yaw and pitch axes [4], [5]. Both phenomena lead to a rapid degradation of the received signal strength and may eventually cause outage conditions. Note that these two effects are relevant even when the UE is stationary.

The above-mentioned effects might severely affect the critical functionality of any communication system with directional antenna – beam tracking. As expected, both blockage and micromobility may lead to outage [6]. The latter refers to the search for an appropriate antenna configuration on both the UE and the BS sides. The beam-tracking procedure can be invoked regularly or on-demand and the search for antenna configurations may occur differently by utilizing either hierarchical or full-scan algorithms [7], [8].

To design mechanisms that alleviate blockage and micromobility impacts, the statistical characteristics of the signal received power (SRP) under these impairments are required. However, owing to the lack of commercial UEs available for these bands, these phenomena have been investigated in isolation. Specifically, measurements of the blockage process conditions over line-of-sight (LoS) and reflected propagation paths at 156 GHz were recently reported in [2] and [9]. Micromobility has been investigated using emulation techniques [5] in the lower millimeter wave (mmWave) band [10]. However, no measurements have been reported for the received signal strength dynamics under the joint impact of both phenomena, and with the beam tracking functionality enabled.

To enable such measurements that contain micromobility and blockage impairments, as well as beam tracking functions jointly at this stage of development of sub-THz/THz equipment, electronic beam tracking capability would be required. However, the implementation of electronic beam steering at frequencies above 100 GHz is accompanied by a number of technological issues. The designs of multi-element radio-electronic devices, such as large phased antenna arrays, which are suitable for microwave and millimeter wave ranges, cannot be easily scaled down and adopted by sub-THz/THz wireless systems. This is primarily due to the very small dimensions of their unit cells, resulting in a significant decrease of the fabrication tolerances for both antennas and tuning elements, enabling amplitude and phase controls. Local irregularities in structural elements eventually lead to distortion of the system characteristics of the arrays. The miniaturization also leads to the increase of AC losses in their layered structures, utilizing dielectric, metallic, and semiconductor elements, due to the skin and proximity effects, eddy currents, parasitic RLC losses and current bypassing. Moreover, widely used CMOS technology becomes less effective at sub-THz/THz frequencies, and the use of A3B5-based devices is needed in 6G real-time beam steering systems. This requires further developments

TABLE 1. Abbreviations utilized in the paper.

Abbreviation	Description
BS	base station
UE	user equipment
THz	terahertz
GHz	gigahertz
SRP	signal received power
VR	virtual reality
3GPP	3rd Generation Partnership Project
LoS	line-of-sight
NLoS	non-line-of-sight
CMOS	complementary metal oxide semiconductor
mmWave	millimeter wave
MCS	modulation and coding scheme
TR	technical report
RAT	radio access technology
NR	New Radio
HPBW	half power beam width
LTE	Long-Term Evolution
SSB	synchronization signal blocks
SNR	signal-to-noise ratio
CSI	channel state information
RLC	radio link recovery
RRC	radio resource control
Tx	transmitter
Rx	receiver
AWG	arbitrary waveform generator
CW	continuous waveform
DAQ	data acquisition system
SINR	signal-to-interference ratio
LMS	least mean squares
EIRP	equivalent isotropically radiated power
URLLC	ultra-reliable low latency service
TB-CNN	time-based convolutional neural networks
TB-RNN	time-based recurrent neural networks

of industrial cleanroom fabrication processes. The technical challenges mentioned above, which will eventually be solved, hamper the design and development of other features of the 6G THz air interface mechanisms, such as statistical tests for discriminating blockage and micromobility events, designing blockage detection algorithms, and improving beam tracking procedures, etc.

The aim of this study is to fill this gap by proposing a received signal strength time-series generation procedure under both dynamic blockage and micromobility impairments, and different types of beam tracking procedures. The ultimate goal of this study was to characterize the dynamics of the signal as perceived by the receiver. To this end, we used the statistical characteristics of blockage and micromobility measurements. The obtained time series can be utilized for the design of various advanced functionalities, such as statistical tests that differentiate between the types of impairments.

The novelty of the work is mainly determined by the absence of SRP data in the sub-THz/THz band, where both micromobility and blockage are simultaneously taken into account. The rationale is the lack of equipment that is capable of performing electronic beam steering at these frequencies. We note that one of the critical goals of our study was to facilitate the development of various mechanisms for 6G



sub-THz/THz communications that require detailed receivedsignal measurements. To this aim, we publicly shared the data-sets reported in our previous study [11]. These traces can be utilized not only to develop physical layer mechanisms but also to confirm complex system models.

The abbreviations used in this paper are listed in Table 1. The main contributions of our work are as follows:

- detailed measurement campaign at the 156 GHz sub-THz band under micromobility and blockage impairments;
- the algorithm for producing semi-synthetic received signal strength traces that accounts for blockage, micromobility, and beam tracking, and the database of synthetic traces generated for different types of beam tracking mechanisms, applications inducing micromobility, and intensities of blockage events;
- observations that: (i) the difference between on-demand and regular beam tracking amounts to 4-6.5 bits/Hz/s and is only relevant for a class of high mobility applications, and (ii) for a large class of applications characterized by low-speed micromobility, the beam tracking interval can be significantly increased from the default 20 ms, allowing the beam tracking overhead to be decreased by up to 20-30 times.

The remainder of this paper is organized as follows. We continue in Section III with a review of related work. Then, in Section III, we report the individual measurements and statistical characteristics of the blockage and micromobility phenomena, which are further utilized to generate synthetic traces. The time-series generation procedure accounting for blockage, micromobility, and the type of beam-tracking procedure is proposed and described in Section IV. The numerical results are presented and discussed in Section V. Finally, the conclusions are presented in the last section.

II. RELATED WORK

In this section, we begin by describing the recent results reported for the measurements and analysis of propagation, blockage, and micromobility phenomena in the sub-THz/THz frequency bands. Then, we will proceed to introduce the types of beam tracking utilized in modern communication systems.

A. PROPAGATION IN SUB-THZ/THZ BAND

The authors in [12] explored the electromagnetic effects caused by the human body, particularly focusing on how it blocks signals in the W-band (75–110 GHz) and G-band (170–260 GHz) through an indoor laboratory environment with an approximate size of 4 × 4 m. A vector network analyzer (VNA) with mmWave extenders and truncated waveguide antennas was employed, with the transmitter and receiver spaced 0,92 m apart, and the blocker's offset varied 0–50 cm from the line-of-sight (LoS). This study analyzes changes in the channel frequency and impulse response when the body obstructs the line-of-sight between the transmitter and receiver during different movements. The results indicate

that the G-band exhibits significantly greater RF attenuation compared to the W-band and that the presence of a blocker introduces new multipath components that can help estimate the target's distance from the line-of-sight. These findings suggest promising developments for enhancing passive radio localization and integrated sensing communication systems.

In [13], a correlation-based time-domain channel sounder was used to conduct channel measurement campaigns in an urban microcell scenario at a frequency of 220 GHz. Measurements were taken at 24 different positions along a university campus road, with distances varying from 34 to 410 m. The analysis focused on the spatial consistency of THz waves and their interaction with the environment, revealing an average additional loss of 16.7 dB due to foliage blockage. Notably, the results indicated a K-factor of 17.5 dB in line-of-sight conditions, which is significantly higher than standard extrapolated values, and showed that an average of 2.5 clusters in the THz band underscores its sparse multipath characteristics, providing valuable insights for future system design in THz communication networks.

Reference [15] presented a beam-tracking algorithm specifically for horn antennas operating at 300GHz, addressing the challenges posed by non-static transmission and reception in wireless communication systems. A measurement campaign utilizing a channel-sounding system was executed to test the algorithm under varying conditions, including both line-of-sight and non-line-of-sight scenarios. The measurements were carried out using a correlation-based time domain channel sounder at Technische Universität Braunschweig, which transmitted a pseudo-random noise sequence with a time resolution of 10.85 ps. In this setup, the transmitter remained stationary while the receiver was mounted on a rail system, enabling angular measurements from 0° to 70° in 5° increments across both line-of-sight and non-line-of-sight scenarios. The results revealed that the algorithm can accurately predict angular changes with a precision of $\pm 1^{\circ}$ for shifts up to 20° , and can extend the tracking range to 70° in line-of-sight and 45° in non-lineof-sight scenarios with slightly reduced accuracy. This study confirmed the effectiveness of the algorithm in real-world situations, paving the way for future exploration of an optimal antenna design for enhanced beam tracking.

The study in [16] focused on analyzing multi-frequency propagation characteristics for mobile services beyond 5G and into 6G, specifically examining frequencies at 28, 38, 71, 82, and 159 GHz in a cubicle office environment. The methodology involved conducting wideband measurements with the transmitter and receiver placed in the same locations, allowing for a direct comparison of path loss, shadow fading, and delay spread across different frequency ranges. The results indicated that while path loss and shadow fading did not significantly vary between 28 and 159 GHz, the delay spread showed a decreasing trend with increasing frequency, suggesting that the existing mmWave propagation models may be applicable to the sub-THz band for path loss and shadow fading but require redevelopment for delay spread.



TABLE 2. Recent studies on sub-THz/THz measurement.

Reference	Frequency	Main findings
Blockage measurement	S	
		Blockage losses range from 6 to 17 dB, with reduced detection times for NLoS scenarios, suggesting antenna
[9] Shurakov A. et al.	156 GHz	beam asymmetry impacts path loss.
	75–110 GHz,	G-band exhibits greater RF attenuation than W-band;
[12] Paonessa F. et al.	170–260 GHz	New multipath components help in estimation distance from LoS
		Blockage causes up to 15 dB attenuation at shorter distances;
		Blockage duration remains consistent – high detection probability (0.96-0.98) was achieved using a novel
[2] Shurakov A. et al.	156 GHz	algorithm.
		Blockage due to foliage causes an average loss of 16.7 dB results also reveal higher K-factor and sparse
[13] Li Y. et al.	220 GHz	multipath in THz band.
Micromobility measure	ements	
		95% confidence in classifying fast/slow micromobility;
[14] Shurakov A. et al.	156 GHz	80% accuracy in distinguishing behaviors over 5 seconds.
		Markov models effectively predict FPT for low micromobility, but overestimate it for controlled environments
[5] Stepanov N. et al.	0.3 - 3 THz	like gaming.
		Beam tracking algorithm accurately predicts angular shifts with a precision of $\pm 1^\circ$ extended tracking range in
[15] Doeker T. et al.	300 GHz	both LoS and NLoS scenarios.
Propagation measurem	ents	
[16] Lee J. et al.	28 – 159 GHz	Path loss and shadow fading are consistent across frequencies, but delay spread decreases with frequency
		Delay spread and angular spread statistics deviate from 3GPP models, indicating the need for updated
[17] Lee J. et al.f	159 GHz	propagation models at sub-THz frequencies.
		10.7 dB increase in path loss for lower receiver heights (LoS);
[18] Ju S. et al.	142 GHz	6.5 dB gain with passive reflecting surfaces.

Additionally, the study included angular domain analyses at 159 GHz, highlighting the influence of narrow beamforming and ceiling reflections on the power distribution, which is crucial for future sub-THz band applications.

The investigation in [17] focused on sub-THz multipath propagation characteristics, specifically at a frequency of 159 GHz, in an outdoor urban environment. Measurements were taken in both Line-of-Sight (LoS) and Non-Line-of-Sight (NLoS) scenarios using a custom-built channel sounder with a 5-GHz bandwidth and a directional antenna setup. Data collection involved 32 LoS points and 46 NLoS points along a typical street in Sejong City, South Korea, with antennas positioned at varying heights and capable of extensive rotational scanning. The study found that the delay spread and angular spread statistics derived from these 159 GHz measurements deviated from the existing 3GPP model parameters, which are only applicable up to 100 GHz, indicating the need for updated models in this frequency range.

The authors in [18] studied sub-terahertz radio propagation measurements at 142 GHz across four factories in New York City to investigate wireless channels for smart factory applications. The methodology involved utilizing a sliding-correlation-based channel sounder with a 1 GHz bandwidth and steerable directional horn antennas at 82 transmitter-receiver locations, analyzing both LoS and NLoS conditions over distances ranging from 5 to 85 m. The experiments yielded over 75,000 directional power delay profiles and established path loss models, revealing that lower receiver heights resulted in increased path loss of 10.7 dB in LOS and 6.0 dB in NLoS scenarios compared to higher receiver placements. Additionally, the use of passive reflecting surfaces demonstrated a significant potential for power gain, showing

an average improvement of 6.5 dB in omnidirectional channel gain, contributing valuable insights for future sub-THz wireless communications in industrial settings.

B. BLOCKAGE PHENOMENON

Dynamic blockage of the propagation path by human bodies is a critical factor that affects the performance of THz communication systems. This phenomenon was first observed in the mmWave domain, where it caused a significant signal attenuation of 15-25 dB, depending on the environment and propagation conditions [19]. As a result, the received signal strength drops drastically, leading to either a downgrade in the modulation and coding scheme (MCS) or a complete outage. Given the even shorter wavelengths of THz signals, the attenuation caused by human-body blockage is expected to be even more severe, posing a significant challenge to the reliability and performance of THz communication systems.

Several methods have been proposed to mitigate human-body blockage in mmWave/THz communication systems. One approach is to utilize non-line-of-sight (NLoS) paths, which can provide continued service during blockages owing to inherent multi-path propagation at these frequencies. Additionally, bandwidth-reservation techniques can support active sessions even when no outage is experienced [20]. However, as noted in the 3GPP TR 38.901 standard, NLoS paths typically generate less than 10% of LoS path power, even at mmWave frequencies. In the event of an outage, the multi-connectivity functionality standardized by 3GPP can be employed [21], [22]. This approach requires the dense deployment of mmWave/THz base stations, which may not be feasible during the initial deployment phase. Combining these approaches, including



multi-connectivity between mmWave and THz radio access technologies (RAT), can still result in a non-negligible probability of session loss owing to blockage. An alternative method is to integrate blockage avoidance techniques into the physical layer using beam focusing [23] and/or non-diffractive beams [24]. However, these studies are still in their early stages of development.

Blockage detection techniques are vital for implementing effective blockage avoidance strategies in mmWave/THz communication systems. These techniques can be classified into two main categories: proactive and reactive approaches [2]. To successfully employ either approach, it is essential to understand the duration of both blockage periods and signal fall and rise times. The signal fall time is particularly crucial as it serves as a key indicator of the type of impairment, allowing for the distinction between blockage and other events, such as fast fading and/or micromobility. Although it cannot be used as a benchmark for development testing, the signal fall time provides valuable insights into the nature of the impairment, enabling the system to respond accordingly. By accurately detecting and characterizing blockage events, communication systems can take proactive measures to mitigate their impact and ensure reliable connectivity.

A notable limitation of the current research on propagation phenomena beyond 100 GHz is the scarcity of studies on the temporal dynamics of the blockage process. For instance, although [25] provides an overview of propagation loss measurements at 140 GHz for various building materials, it does not report the characteristics of the blockage process. Similarly, the authors of [26] and [27] reported attenuation values for 300 GHz in the context of vehicular blockage, but these findings are not directly applicable to human body blockage owing to differences in materials and geometries. In contrast, numerous studies have investigated the transparency characteristics of materials [25], [28]. For example, [25] examined the attenuation induced by various materials in the sub-THz range, whereas [28] presented measurements at four different frequencies, including two in the sub-THz range. Furthermore, [29] proposed an analytical model based on the average blockage probability, which was estimated empirically as a function of the relative positions of the receiver and transmitter, average heights, antenna parameters, and room size.

In general, despite the availability of data on sub-THz signal penetration through various materials and measurement campaigns for vehicular communications, there is a significant gap in the comprehensive characterization of the human body attenuation within the sub-THz frequency spectrum. This knowledge gap is particularly concerning with regard to signal fall and rise times, which are crucial for understanding the dynamics of the blockage process.

C. MICROMOBILITY PHENOMENON

The influence of micromobility is particularly relevant in systems that employ directional antennas. Although 5G

New Radio (NR) systems currently use directional antenna patterns, the half-power beam width (HPBW) of these antenna arrays is relatively broad, which might not immediately suggest a significant impact from micromobility. However, as reported in [10], experimental evidence has been presented indicating that micromobility can indeed cause a decrease in the received signal strength, particularly within 5G NR networks. As we transition to higher-frequency bands, such as the THz band, the antenna arrays become more compact, providing a higher density of elements and potentially causing a decrease in the HPBW, along with directional sensitivity. The pioneering research on the effect of user micromobility on link performance was detailed in [30], where researchers employed smartphone sensors, such as gyroscopes and accelerometers to study the unpredictable movement patterns of the beam's apparent direction. This study highlights a fundamental tradeoff between outage probabilities and spectral efficiency based on different HPBW values.

The authors of [4] conducted a micromobility emulation study using a laser pointer attached to a smartphone to represent the direction of the beam. They analyzed four types of applications (video watching, VR watching, racing games, and phone calling) and found that each type has distinct micromobility characteristics. They also discovered that some applications, such as video watching and phone calling, can tolerate longer intervals between beam-tracking updates. Leveraging statistical insights from [5], researchers introduced and calibrated three distinctive models: a complex two-dimensional Markov model, and two simpler one-dimensional models - both projecting behavior over the Oy and Ox axes. The accuracy of predicting an outage event following a beam adjustment was the highest with the two-dimensional Markov model, despite its intricate nature due to numerous states. Simpler decomposed models acted as adequate first-order approximations for non-interactive applications, excluding racing games where user control is pivotal.

Understanding the nuances of micromobility prompted further inquiry into its impact on both user experience and system performance, alongside the development of remote application detection techniques. A [6] study highlighted how micromobility influences the outage performance in advanced 6G THz communications, demonstrating that reducing the beam search time by one-tenth through faster antenna transitions could optimize the trade-off between outages and spectral efficiency. Another investigation in [22] explored the collaborative deployment of mmWave and 6G THz systems, concluding that reliable fallback options, such as 4G LTE, are beneficial in environments with sporadic connectivity owing to micromobility.

To refine remote application detection and optimize beam-tracking durations, researchers in [31] advocate using gyroscopes and accelerometers to curtail the search space for antenna orientations at both Base Stations (BS) and User Equipment (UE). Nonetheless, the current limitations in



sensor precision pose challenges in achieving gains in beamsearching efficiency. An alternative strategy highlighted in [32], centered on identifying the boresight of the main lobes, showed potential for near-perfect application identification, thus determining optimal beam intervals. However, reliance on boresight coordinates, which are unavailable to both the BS and UE, restricts their practical applicability. Despite significant advancements, a definitive method for quantifying the influence of micromobility on the signal strength after beam adjustment remains unrealized.

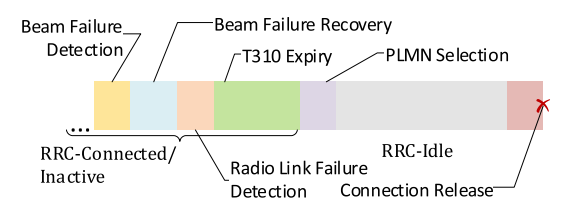


FIGURE 1. Beam failure management in 5G NR.

The researchers in [14] investigated the impact of micromobility on beam tracking for 5G/6G systems operating in the sub-THz frequency band at 156 GHz. A multistage measurement campaign was conducted to collect the received signal strength traces from four popular smartphone applications (voice calling, video watching, VR, and gaming). The methodology involved a multi-stage measurement setup to emulate the user equipment beam center micromobility, beginning with a laser pointer attached to the UE to track motion on a screen. In the second stage, field measurements were conducted at 156 GHz using a testbed, where goniometers were parameterized with transmitter antennas to replicate the movement of the UE's beam center, while a fixed receiver acted as the base station. The received signal patterns were analyzed using statistical Mann-Whitney tests and machine learning techniques, such as random forests, to classify applications based on their micromobility characteristics (fast vs. slow). The results show that the Mann-Whitney test can classify application types with 95% confidence within 1 second, while random forests achieved 80% accuracy in distinguishing fast and slow micromobility behaviors over 5 seconds. This approach provides a way to estimate optimal beam tracking intervals without additional signaling, improving the efficiency of mmWave and sub-THz systems.

A summary of recent sub-THz/THz propagation, blockage, and micromobility measurements and modeling efforts is provided in Table 2.

D. BEAM TRACKING

Generally, beam-tracking procedures utilized in modern systems with directional antennas differ in two aspects: (i) when the search for an optimal antenna configuration is initiated and (ii) how the search is performed. The former property leads to two instances of beam tracking: regular and on-demand. Regular beam tracking, which is currently

utilized for 5G NR systems, scans for optimal antenna configurations over regular time intervals (set at the BS side to 10-320 ms via the frequency of Synchronization Signal Blocks (SSB), as defined in TS 38.211 [33]). According to the on-demand beam-tracking approach, the BS and UE initiate beam searching only when outage conditions occur, that is, the received signal strength falls below the sensitivity of the UE.

Once a beam search is initiated, either a hierarchical or full scan can be performed [7]. In the first case, the time taken to determine the alignment is $T_H = (N_B + N_U) \delta$, where δ is the array switching time (2-10 μ s for modern antenna arrays), N_B and N_U are the number of antenna elements at the BS and UE, respectively. In the case of a full scan, the time complexity is significantly longer, and is given by $T_F = (N_B N_U) \delta$. Note that the hierarchical search procedure limits the coverage of the BS, as during the beam searching, one of the sides, the BS and UE, is successively placed in an omnidirectional regime, thus reducing the antenna gain.

Both blockage and micromobility may lead to the degradation of the received signal strength. Once the effective SNR falls below the threshold defined by the lowest MCS, the UE begins receiving beam failure instance indicators from the physical layer via the SSB or Channel State Information (CSI) reference signals. As the number of indicators reaches a pre-configured threshold, beam failure is detected [34], as shown in Fig. 1. Having detected the failure, it initiates beam failure recovery attempting to fetch the beam with the highest SNR. In the case of micromobility, the UE typically switches to another available beam and restores its connection. However, in the case of blockage, there might be no beams available with a sufficient SNR. The UE then starts a Radio Link Recovery (RLC) procedure [35]. Upon receiving n310 consecutive "out-of-sync" indications from the lower layers the UE starts timer t310 [36]. As the t310 timer expires, the UE moves to the RRC-Idle state and begins the network selection procedure until a suitable cell is found.

III. MEASUREMENTS AND CHARACTERISTICS

In this section, we outline the experiments utilized to obtain traces of the received signal strength under blockage and micromobility in isolation, and report their statistical characteristics utilized in the proposed trace generation procedure. The notation used in this study is listed in Table 3.

A. BLOCKAGE

1) MEASUREMENTS SETUP

We used the measurements presented in [2]. To collect empirical data on human body blockage attenuation, the authors conducted a large-scale measurement campaign, as shown in Fig. 2. They utilized a sub-THz transmitter (BS) operating at a carrier frequency of 156 GHz with an emitted power of 90 mW. Both the BS and receiver (that is, UE) were equipped with pyramidal horn antennas. The BS and UE



TABLE 3. Notations.

Notation	Description
N_U	number of UE antenna array elements
N_B	number of THz BS antenna array elements
T_H	hierarchical beamsearching duration
T_H	full-scan beamsearching duration
δ	array switching time
Δ	channel sampling resolution
x	BS-to-UE distance
d	BS-to-blocker distance
h	BS/UE height
s_G	goniometer nominal scan

half-power beamwidths were 8-10° with gains of 25-28.4 dB. The BS and UE antennas were aligned at all times during the experiment. The time constant of the UE signal amplification stage was set to 30 μ s. The channel-sampling resolution was $\Delta = 50\mu$ s.

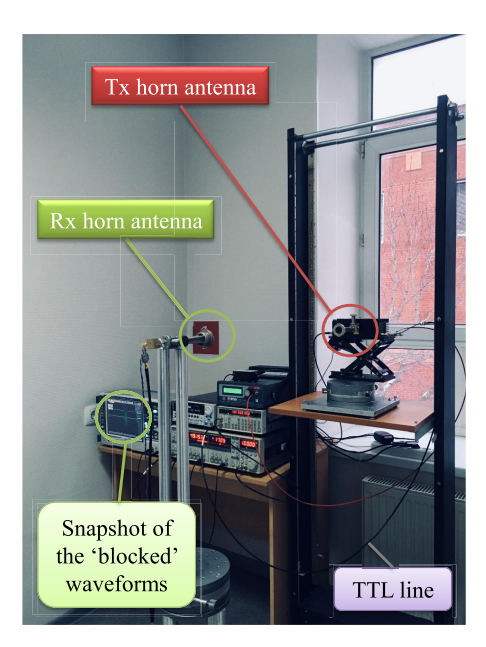


FIGURE 2. Illustrations of equipment for blockage measurements [2].

The measurement campaign was carried out in an empty hall with length 7.5 m, width 4.5 m, and height 3 m. The BS-to-UE distances were set to 3, 5, and 7 m. The authors considered a blocker crossing the LoS at a standard walking speed of 3.5 km/h. They utilized multiple BS-to-blocker distances, denoted by d, for each BS-to-UE distance, denoted by x: (i) x = 7 m: d = 1.5, 3.5, 5.5 m, (ii) x = 5 m: d = 1.5, 2.5, 3.5 m, and (iii) x = 3 m: d = 1.5 m. Finally, two BS and UE heights were considered: d = 1.35 m, corresponding to the LoS blockage by a chest, and d = 1.65 m, corresponding to the head blockage.

2) STATISTICAL CHARACTERISTICS

An illustration of the typical received signal strength for two BS-UE heights (1.33 m and 1.65 m) is provided in Fig. 3. Here, we observe that the signal does not drop immediately,

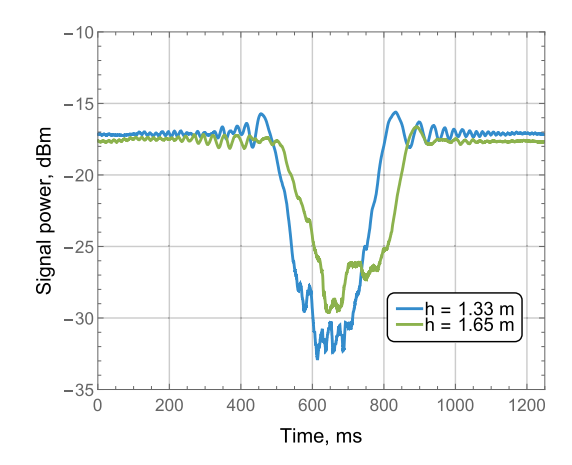


FIGURE 3. Received signal power under blockage.

allowing the system to detect and react to the blockage event. In addition, the profile at the head BS-UE level is slightly different from that at the chest level with attenuation being 2-4 dB less. However, these differences are not related to the signal fall periods, which primarily affect the system under blockage conditions. This means that in terms of blockage avoidance techniques, similar algorithms can be utilized for different heights where the LoS is crossed by the human body.

The statistical characteristics utilized further in the proposed algorithm are shown in Table 4 for the BS and UE heights of 1.65 m. As one may observe, these time-dependent characteristics, including the signal fall, rise, and blockage time (note that the blockage time here includes fall and rise times), vary slightly for different BS-UE distances. However, as can be observed, BS-UE height has significant impact. The rationale is that a height of 1.65 m roughly corresponds to the head while 1.33 m – to the chest. Thus, one may see significantly higher variability in the time-related characteristics and attenuation for 1.65 m height.

TABLE 4. Basic statistics on blockage characteristics.

UE height	1.33 m			1.65 m				
BS-UE distance	3 m	5 m	7 m	3 m	5 m	7 m		
	Mean values							
Attenuation, dB	22.53	22.35	18.26	16.61	15.72	14.99		
Rise time, ms	93.11	97.01	99.36	117.5	124.0	134.9		
Fall time, ms	158.6	162.4	176.7	124.2	136.1	165.1		
Block. time, ms	674.0	684.0	839.2	877.5	881.5	893.3		
		Standard	deviation			•		
Rise time, ms	12.83	24.83	38.22	57.57	59.21	56.67		
Fall time, ms	9.45	22.75	40.68	39.92	57.89	62.34		
Block. time, ms	13.52	20.63	47.18	53.40	53.70	56.67		
Bl. power, dB	1.89	1.87	1.13	1.04	1.09	0.95		
N-bl. power, dB	.025	.025	.027	.027	.025	.026		

B. MICROMOBILITY

1) MEASUREMENTS SETUP

As miniaturized equipment operating in the sub-THz frequency band is still missing, we utilized a multi-step



methodology to measure the realistic behavior of the received signal strength under micromobility impairments.

We begin with the emulated behavior of the main lobe boresight of the antenna radiation pattern reported in [5], where the authors considered four types of applications: (i) video watching, (ii) phone calls, (iii) VR watching, and (iv) racing game. Note that the latter two are characterized by a fast micromobility speed, whereas the former is an example of an application with a low micromobility. Phone calling falls in between these two extremes. By utilizing the available statistical data, we produced two-dimensional (2D) Markov models as described in [4] for each application by dividing the entire area of the screen into multiple rectangles of equal size and considering each of them as the states of the model. The transition probabilities between states were then computed. These models were further utilized to generate traces corresponding to the micromobility of each application.

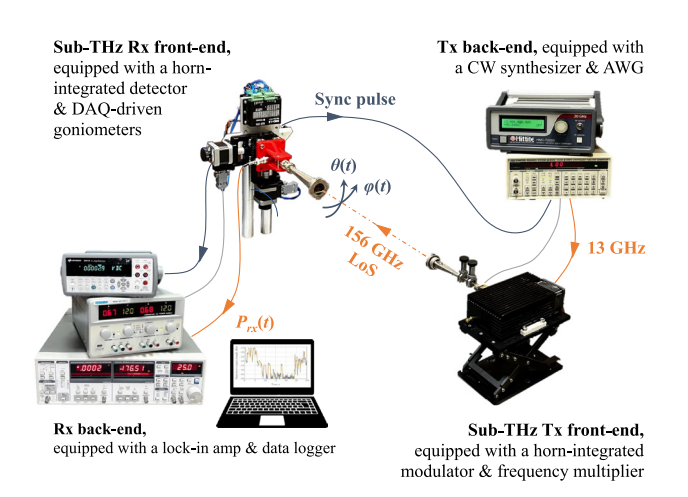


FIGURE 4. Schematic diagram of the measurement setup.

To obtain empirical traces of the received signal strength, laboratory equipment operating at 156 GHz was used. The measurements were conducted in conventional office premises 5.5 m in length, 5.2 m in width, and 3 m in height. The office was filled with tables, shelves, and chairs located along the perimeter. They did not significantly impact the LoS (and close to that) communications compared to the unfurnished case, since the antennas of wireless modules had a gain of 25-28.4 dB. We also eliminated the impact of standing waves due to multiple signal reflections and scattering off measurement setup elements by using a radio-absorbing material. To exclude notable variations in atmospheric absorptance and thermal drifts in electronics, a constant temperature and humidity were maintained in the office during the measurements. The human impact on measurement reproducibility was eliminated by implementing software-driven hardware emulation of user biomechanics. Dozens of independent measurements were conducted to ensure high statistical relevance of empirical data.

The frequency choice is justified by the existence of the atmospheric transparency window with pronounced absorption peaks at 119 GHz and 184 GHz. It ensures efficient distribution of radio signals in the beyond-100-GHz channels of the International Mobile Telecommunications of 2030 and beyond (IMT-2030) [37] in both low and high humidity air environments [38]. Moreover, the study does not benefit noticeably from changing the operating frequency within the chosen atmospheric transparency window, since the propagation and scattering of radio waves in this frequency range are qualitatively consistent. Going to even higher frequencies is rather impractical because of a gradual decrease in the output power and sensitivity of sub-THz/THz solid-state transmitters and receivers.

The employed sub-THz transmitter (Tx) and receiver (Rx)were placed 4 m apart at the same height. A schematic diagram of the measurement setup is shown in Fig. 4. The Tx offers a modulated continuous waveform (CW) with an output power of 44 mW. An arbitrary waveform generator (AWG) was employed for modulation control. A diode detector with responsivity of 100 V/W was used on the Rx side with the system noise equivalent power about 1 nW/ $\sqrt{\text{Hz}}$. To dynamically change the orientation of the Rx (i.e., UE) antenna on the yaw (vertical) and pitch (transverse) axes, a 2D goniometer driven by a data acquisition system (DAQ) was utilized. The DAQ also synchronizes the movement of the goniometer with the generation and processing of the sub-THz signal. The nominal scan speed of the goniometer was $s_G = 6.67$ °/s per axis. To parameterize the goniometer system, we utilized the beam center emulation data provided in [5] for the four considered applications obtained as discussed above. As some of the applications were characterized by speeds higher than s_G , the original time of compression/decompression was utilized.

2) STATISTICAL CHARACTERISTICS

A total of 30 individual time series were obtained for each application. The typical behavior of the received signal strength for the first 30 s and the first 1 s is shown in Fig. 5. Observe that, under regular beam tracking, the beginning of the trace indicates behavior that occurs immediately after beam alignment. As one may observe, watching video and phone calling applications are indeed characterized by slow micromobility because the received signal strength remains intact for a few seconds after the beam tracking time instant. On the other hand, VR watching and racing game lead to dramatic degradation of the received signal strength by more than 15 dB in just a few hundred milliseconds. However, even this time span is much longer than the maximum beam tracking interval in the 5G NR standard, which is set to 320 ms. Thus, for both classes of applications significant resource and UE energy savings could be achieved.

One critical parameter for various outage avoidance techniques, such as the multi-connectivity option [39], is time signal fading to a given level. This metric is illustrated



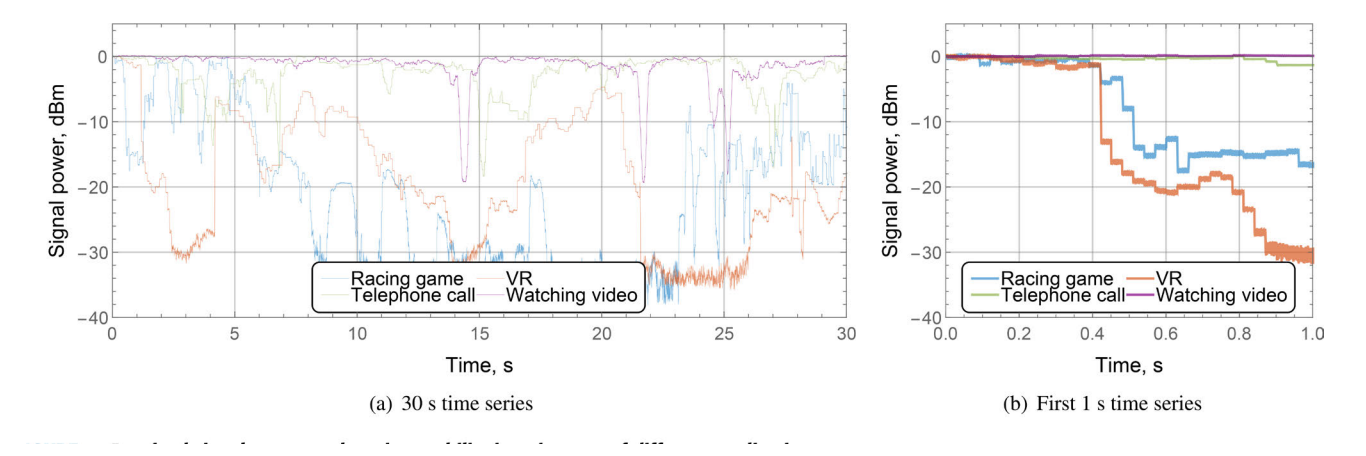


FIGURE 5. Received signal power under micromobility impairments of different applications.

in Table 5 for different types of applications and two considered beam-tracking options, where N/A indicates that no outage was detected. The minimum signal-to-interference ratio (SINR) threshold was set to that of 5G NR standards at 8.7 dB. For on-demand beam tracking, these data were obtained directly by averaging the time to fall for all the measured time series. For regular beam tracking, these metrics were calculated for the maximum beam-tracking interval of 320 ms. Thus, in this case, only the first 320 ms in each time series was considered.

TABLE 5. Mean signal fall time to a given threshold (in seconds).

Regular beam tracking							
S_{th} , dB	Racing	Phone	VR	Video			
3	1.77	1.83	2.10	1.88			
5	1.78	1.85	2.11	1.90			
7	1.80	1.87	2.13	1.92			
10	1.83	1.89	2.16	1.94			
15	2.26	6.42	2.69	2.13			
Time to outage	N/A	N/A	N/A	N/A			
On-demand bea	On-demand beam tracking						
3	0.57	1.75	0.42	1.83			
5	0.57	1.77	0.42	1.85			
7	0.60	1.79	0.42	1.86			
10	0.60	1.89	0.42	1.89			
15	0.75	2.02	0.48	2.11			
Time to outage	12.71	N/A	1.13	N/A			

From the data presented in Fig. 5 and Table 5, we see that micromobility alone rarely leads to a loss of connectivity. For regular beam tracking with a 320 ms interval, this never occurs for any considered application. For on-demand beam tracking outage is observed for only "fast" micromobility applications such as racing game and VR watching. However, even for these applications, the time until the outage is rather large. However, note that these conclusions depend heavily on the received signal strength immediately after the beam tracking time instant, which is dictated by the distance between the UE and BS, as well as the emitted power and

antenna gains on both sides of the communications link. Thus, for larger separation distances, micromobility may lead to outages.

IV. SYNTHETIC TRACES GENERATION

In this section, based on the statistical characteristics of the individual blockage and micromobility measurements reported in the previous section, we describe the time-series generation procedure that simultaneously accounts for the blockage, micromobility, and type of beam tracking utilized by the system. We note that blockage and micromobility processes are widely assumed to be independent [40], [41] as small rotations and shifts of device in user's hand are generally guided by the user behavior [42] rather than being affected by external objects.

The overall methodology utilized in our paper to generate traces and evaluate the metrics of interest is illustrated in Fig. 6. We specifically note that different from other studies, our approach allows one to produce combined traces with blockage, micromobility, and beamsearching effects which is provided by "trace-generation" and "outage identification" stages of our methodology.

The overall procedure for producing traces with both blockage and micromobility impairments is deterministic for the both on-demand and regular beam tracking options. The former is always (i) beam tracking, (ii) micromobility affecting the received signal power continuously and (iii) blockage affecting the received signal strength abruptly. If micromobility or blockage leads to an outage prior to the next beam tracking time instant, beam tracking is immediately invoked. Otherwise, beam tracking is invoked at a preplanned time instant. For on-demand beam tracking, an outage always invokes beam alignment. Thus, there is no need for more advanced data processing when producing traces containing both types of impairment.

The overall state-generation procedure is illustrated in Fig. 7. The procedure is basically a superposition of blockage and micromobility processes based on their statistical



Data collection Blockage Micromobility Retrieve samples of SRP for human-Retrieve samples of SRP for different body blockage applications Preprocessing Blockage Micromobility 1. Smooth data using moving average Smooth data using moving average 2. Extract roundtrip times for signal 2. Identify blockage event timestamps (waving, falling, raising) for each sample power (from zero to zero attenuation) 3. Calculate event duration and signal 3. Calculate roundtrip duration and power fluctuation statistics (mean and signal power fluctuation statistics deviation) (mean and deviation) Trace generation **Blockage** 1. Generate exponentially distributed intervals between blockages 2. Add randomly generated blockage events using collected stats 3. Fill the traces with event-defined fluctuations using collected stats Micromobility 1. Generate attenuation caused by beam misalignment based on collecte stats 2. Impose attenuation on top of blockage process Outage identification and beamsearching Periodic beamsearching On-demand beamsearching Add periodic beamsearching periods Identify outage periods Add periodic beamsearching periods and beam alignment syncpoints and beam alignment syncpoints Postprocessing: collect outage and signal power stats

FIGURE 6. Trace-generation methodology.

characteristics with appropriate adaptation of the received signal strength interrupted by beam-tracking procedures. In the first stage, we calculated the statistical characteristics of blockage and micromobility traces. The pre-calculated values of these characteristics are listed in Tables 4 and 5, respectively. The actual trace generation is then initiated at time t=0 in the non-blocked state, assuming that beam searching has just occurred. In this step, we additionally initialize the variable responsible for the time to blockage, which can be approximated using an exponential distribution [6], [43].

In the proposed approach, we considered the signal strength obtained from the blockage process as the reference signal power. To model the process, we generated exponentially distributed intervals between subsequent blockages. Within these LoS intervals, we imposed synthetic fluctuations that followed a normal distribution with the mean and standard deviation parameter values previously estimated during the measurement campaign. To properly collect the data, we first applied the moving average with parameter $\epsilon =$ 0.01 to remove the noise caused by receiver hypersensitivity. This allowed us to fetch the fluctuations extrema and compute the time intervals between them. The blockage phenomenon was considered as a 5-phase sub-process comprised of (i) ingress fluctuations, (ii) fall period, (iii) stabilization period, (iv) rise period, and (v) egress fluctuations. All phases similarly followed a normal distribution with parameters obtained within the measurement campaign.

In addition to the signal power produced by the blockage process modeling by selecting the application type, we specify the slope of the signal fall caused by the micromobility process. This was performed assuming independence of the micromobility and blockage processes by applying least mean squares fitting (LMS) to the slope of the micromobility pattern, as shown in Fig. 5. The obtained averaged slope was then superimposed with the received signal strength processes modeled by the normal distribution with the standard deviation presented in the last row of Table 4. If regular beam tracking is used, the process is restarted after a certain beam-tracking time interval, and the procedure is repeated. Note that the process is delayed by the beamsearching time provided in Section II, depending on the type of searching procedure utilized, hierarchical or full scan. During this procedure, the received signal strength is set to the outage level. The procedure is restarted if an outage occurs prior to the expiration of the beam-tracking interval. When on-demand beam tracking is used, the process continues until the outage condition is reached, and then restarted.

Note that blockage may occur during divergence from the initial received signal values at time t=0 as a result of micromobility. Once the non-blockage time expires, the characteristics of the blockage fall time and mean attenuation are utilized to calculate: (i) the additional slope induced by the signal fall as a result of blockage and (ii) the level it reaches in the blocked state. During the signal fall time, both slopes were added and utilized to calculate the mean value of the received signal. The non-blocked standard deviation is still utilized to account for the fast signal deviations around the mean. Once the blockage state was reached, the standard deviation corresponding to the blockage state was used. A similar procedure was used to determine the signal rise time.

We also note that when on-demand beam tracking is utilized, the link is lost and no connection is available, that is, signal received power is not defined during the beam searching time. Alternatively, when regular beam tracking is used, the connection is still up during the beam searching time. However, since we create traces for further research activities, to clearly indicate the time intervals, when beam searching is performed, we utilize the constant value of the signal received power, $-100 \ \mathrm{dB}$.

It should also be noted that the traces produced do not account for many properties of the real-world environment, such as interference, simultaneous blockage by multiple objects, possible reflections, non-linear motion, and device power management techniques. The proposed procedure results in approximate (e.g. qualitative) signal strength behavior, as observed at the UE or BS side. Nevertheless, it retains the principal properties measured in practice and can thus be utilized for the development of different performance improvements for future 6G sub-THz/THz systems.

Fig. 8 illustrates the differences between traces with micromobility impairments only, blockage impairments only, and joint impairments. Here, we utilize VR watching as the application of interest. As one may observe for



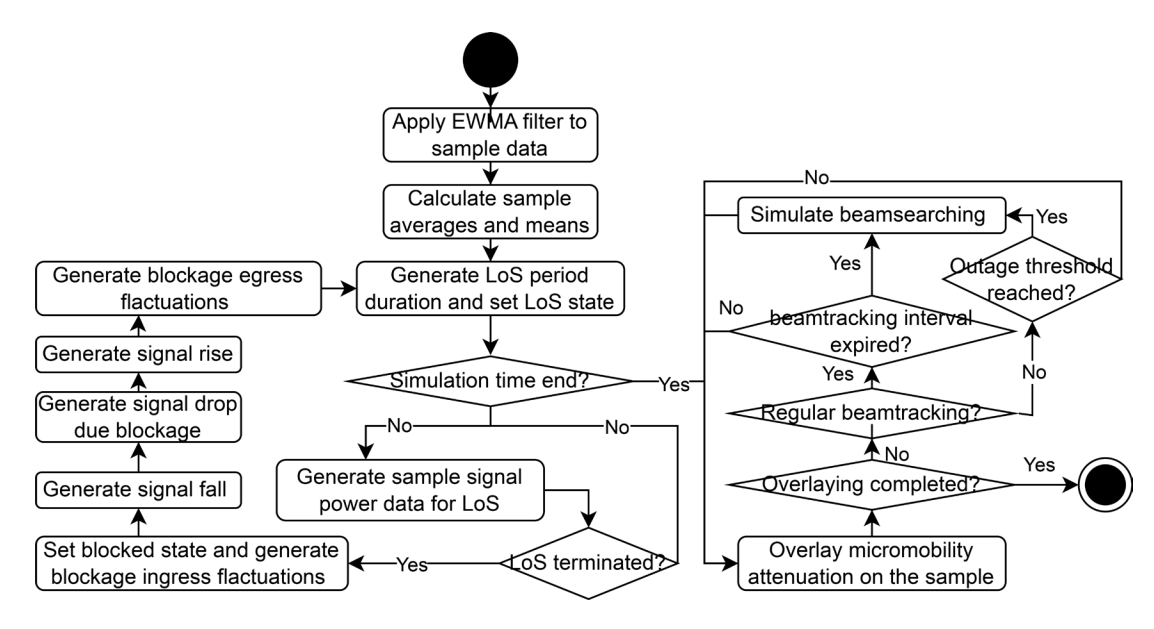


FIGURE 7. Synthetic trace generation algorithm.

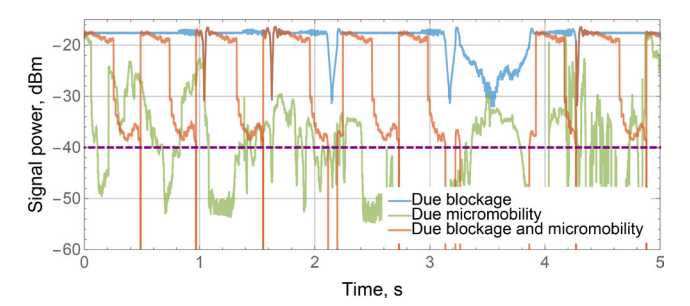


FIGURE 8. Comparison of different types of traces.

considered distances, blockage alone does not lead to the loss of connectivity. The impact of micromobility may however be more profound. The time series representing joint impairments have higher variability.

V. NUMERICAL RESULTS

In this section, we present the results of the proposed trace synthesis procedure and characterize the statistical properties of the generated traces. The default system parameters used in this study are listed in Table 6. Recall that we also utilized the statistical parameters of the blockage and micromobility processes from Tables 4 and 5, respectively, as described in Section IV. We also assumed a fixed-value threshold for outage conditions. As such parameters are usually vendor-specific, we fetched the difference in SNR between the highest and the lowest MCS (29 dBm) proposed in [44]. Then, we transposed this difference onto the reference SNR of the available blockage process measurements (-11 dBm) and finally obtained the threshold of -40 dBm.

A. SYNTHETIC TIME SERIES

We began by observing the behavior of the generated synthetic time series illustrated for on-demand and regular

TABLE 6. Default system parameters.

Parameter	Value
Carrier frequency	156 GHz
Bandwidth	2 GHz
BS antenna array	16×16 el.
BS-to-UE distance	7 m
beam tracking procedure	on-demand/regular
Beamsearching type	hierarchical/full scan
Antenna switching time	10 μs
Applications	VR/video/gaming/calling
Blockers density	0.1 bl/m^2
Blockers radius	0.3 m
Blockers height	1.7 m
Outage threshold	-40 dB
Regular beam tracking interval	320 ms

beam tracking, as shown in Fig. 9, where we considered three beam-tracking intervals: 80 ms, 320 ms, and 1000 ms. By analyzing the presented illustrations, one may observe that setting the beam-tracking interval to a rather small value of 20 or 80 ms almost fully avoids drastic signal drops as only a few are visible in Fig. 9. In general, the received signal strength in this case was maintained at a very good level and barely deviated from the time instant immediately after beam alignment. Extending this interval first to 320 ms and then even further to 1000 ms, we observe that deviations become more impactful, especially for high speed mobility applications, such as VR watching and race gaming. The joint effect of blockage and micromobility impairments can be more than 30 dB, even at the short distances considered in our study. As expected, for on-demand beam tracking, we have much larger variations since the procedure is performed only when the connection is lost. Remarkably, even high-speed mobility applications rarely experience outage conditions. Note that this is primarily due to the considered short



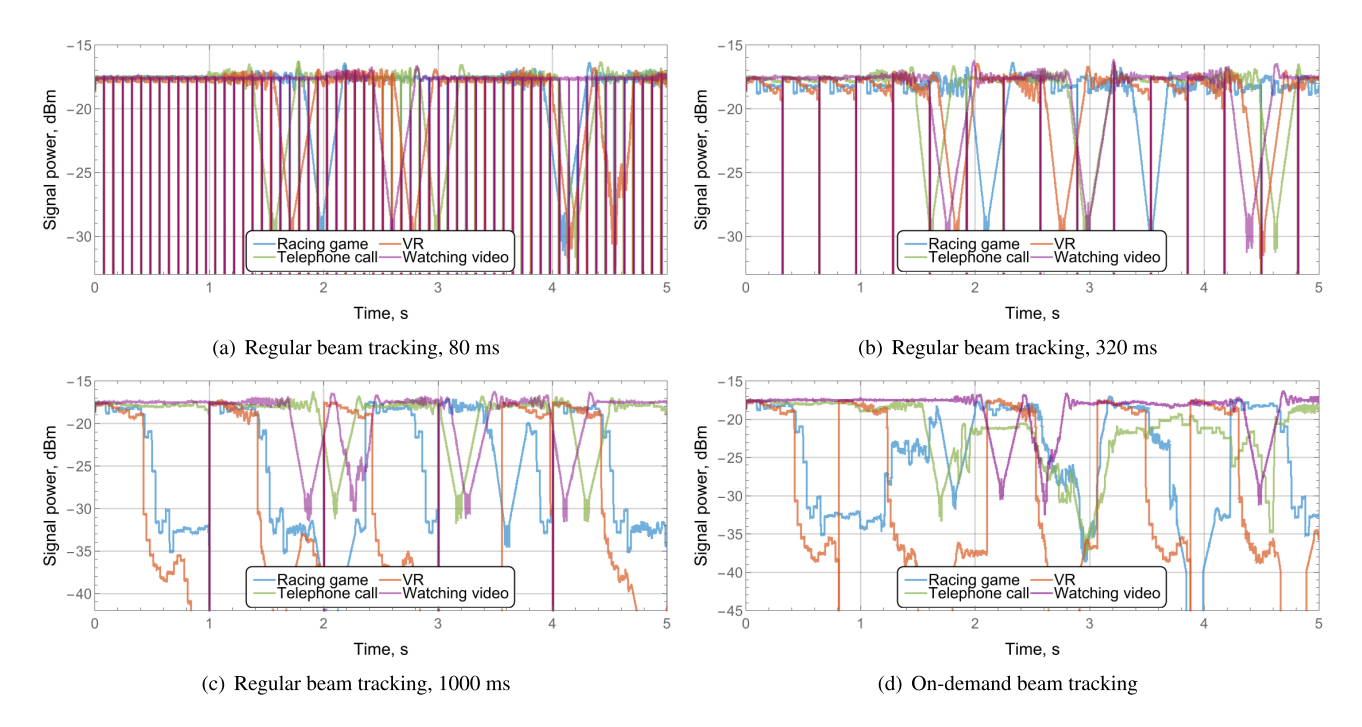


FIGURE 9. Received signal power under blockage and micromobility impairments for different applications and beam tracking procedures.

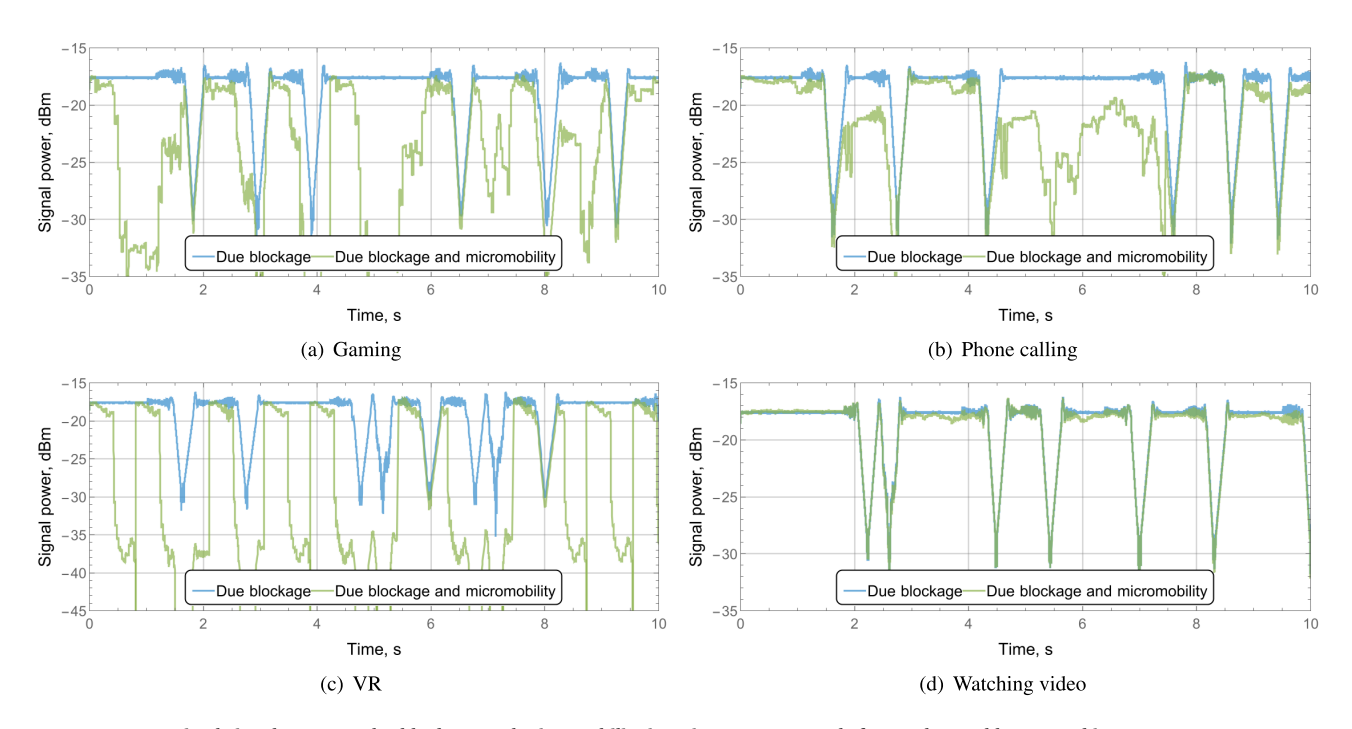


FIGURE 10. Received signal power under blockage and micromobility impairments separately for on-demand beam tracking.

distances, which allow the maintenance of the received signal strength at high values.

We also observe that either micromobility or blockage alone rarely leads to outage, and it is always the joint effect of blockage and micromobility which cause the loss of connectivity. To support this observation in Fig. 10 and 11, we demonstrate the attenuation caused by blockage

and micromobility impairments occurring separately for on-demand and regular beam-tracking algorithms, respectively. Here, we see that depending on the application type either micromobility or blockage can be the dominating factor responsible for outage. Recall, that as different actions need to be performed to alleviate the impact of these impairments (e.g., use of multi-connectivity [39] in the case of blockage or



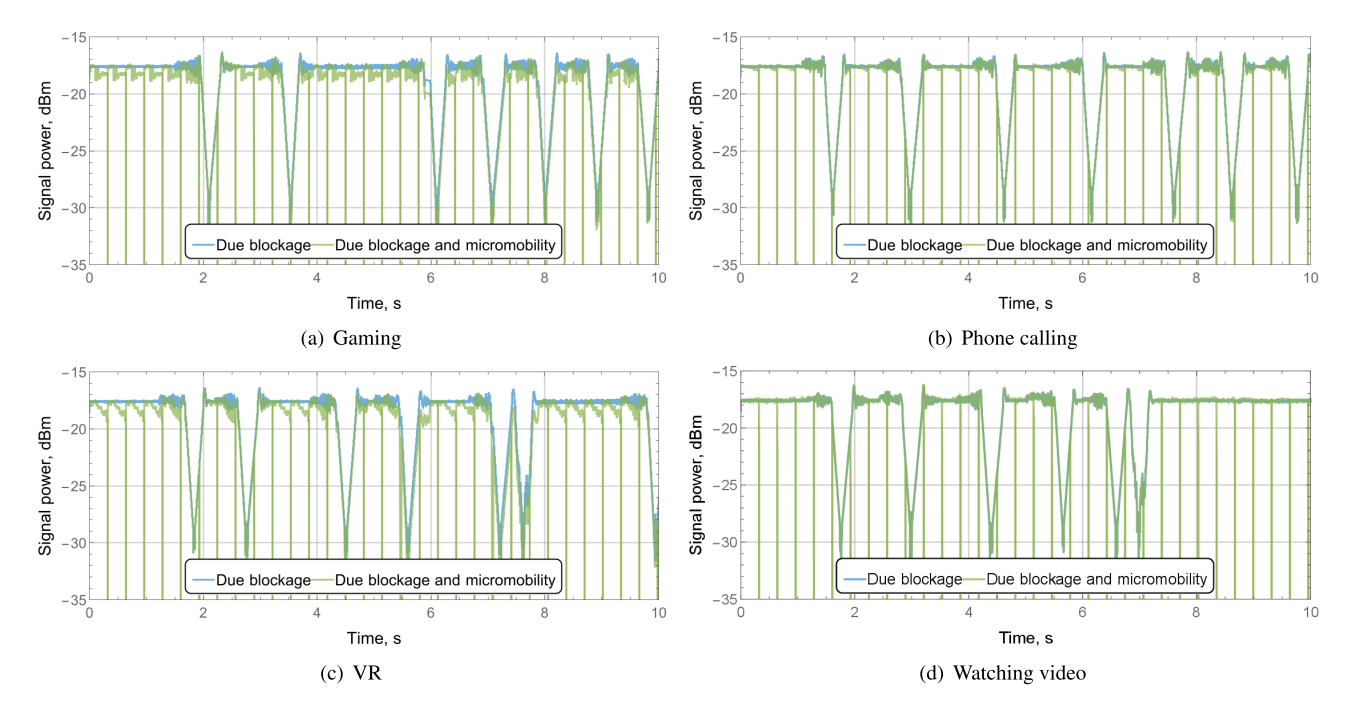


FIGURE 11. Received signal power under blockage and micromobility impairments separately for regular beam tracking with 320 ms interval.

initiating beam-alignment procedure) differentiating between the reason for outage is critically important. Second important thing is that both proactive and reactive blockage-detection techniques developed in the past [2], [3], [45], [46] do not account for presence of micromobility impairments in traces. Thus, another critical task is to adapt those algorithms to the realistic conditions where both types of impairment are present.

B. STATISTICAL CHARACTERISTICS

We now analyze the statistical characteristics of the generated traces. To this end, Table 7 demonstrates the mean signal fall time to a given threshold of {3, 7, 10, 15} dB for different applications, and identifies the associated favorable and unfavorable beam tracking periods. Specifically, the columns marked with "Per." show the best (in case of favorable) and worst (unfavorable) periods, while columns to the left of "Per." shows the fall time for the applications. Here, we considered the following standardized beam-tracking intervals {20, 80, 160, 320, 1000, 2000} ms. The results show that for applications with high-speed micromobility, such as VR watching and race gaming, the best options are 320 and 80 ms, respectively, whereas for low-speed applications, a period of 1000 ms is sufficient. However, video watching is only slightly affected by beam tracking resulting in a less than 15% difference between the best and worst periods. In addition, one may observe that regular beam tracking generally allows for extended fall times compared to on-demand beam tracking throughout all considered periods. Observe that if the information about the type of application is available to the UE and BS sides, this would allow a decrease in the overhead required for beam tracking by up to 20-30 times.

TABLE 7. Mean signal fall time in seconds for different applications and different periods of regular beam tracking.

Regular beam tracking								
S_{th}	Race	Per.	Phone	Per.	VR	Per.	Video	Per.
dB	S	ms	S	ms	S	ms	S	ms
Favo	rable be	am trac	king peri	ods				
3	1.206	80	1.219	1000	1.221	320	1.185	20
7	1.249	80	1.265	1000	1.271	320	1.229	20
10	1.351	80	1.318	320	1.328	320	1.311	20
15	∞	N/A	∞	N/A	∞	N/A	∞	N/A
Unfa	ivorable l	beam tı	acking pe	eriods				
3	0.466	2000	0.765	2000	0.416	2000	1.087	80
7	0.522	2000	0.809	2000	0.431	2000	1.096	320
10	0.557	2000	1.207	2000	0.443	2000	1.154	320
15	0.674	2000	4.176	2000	0.504	2000	∞	N/A
On-o	On-demand beam tracking							
3	0.366	N/A	0.855	N/A	0.379	N/A	1.123	N/A
7	0.430	N/A	0.972	N/A	0.394	N/A	1.175	N/A
10	0.504	N/A	1.115	N/A	0.405	N/A	1.225	N/A
15	0.791	N/A	2.256	N/A	0.501	N/A	6.388	N/A

Furthermore, Table 8 demonstrates the mean attenuation measured in dB with respect to time t=0 for different applications and beam-tracking settings, including the type of beam-tracking procedure and time interval between beam-tracking time instants for regular beam tracking. We observe that the principal difference between the average channel quality degradation is observed only for the most dynamic racing game and VR applications under long beam-tracking periods (1000 and 2000 ms). Here, the



difference between on-demand beam tracking and regular beam tracking with a 20 ms time interval is more than 6 and 4 dB, respectively. For the currently utilized MCSs in 5G NR [33], this may result in a 4-6.5 bits/Hz/s degradation in spectral efficiency. As the time interval increased to 2000 ms, a difference of up to 15 dB was observed. For slow micromobility applications such as phone calling and video watching, there is no difference between on-demand and regular beam tracking, as well as between regular beam tracking with different time intervals, as the average signal attenuation for all the considered cases is between 2-3.5 dB.

Note that in 5G NR, regular beam tracking is exclusively utilized to keep the connection up all the time. However, the authors in [8] demonstrated that under specific conditions for systems with extremely directional radiation patterns (specifically, for HPBW less than 0.1°) in the presence of micromobility, on-demand beam tracking is characterized by higher spectral efficiency. However, by analyzing the reported results demonstrated in Table 8, we see that this is not the case for applications characterized by high micromobility speeds (e.g., racing game and VR watching). The rationale is that between blockage time instants, micromobility is the dominant factor responsible for the received signal strength attenuation, and it results in a much higher mean attenuation for these applications when on-demand beam tracking is used compared to regular beam tracking. However, for some applications when the UE is not severely affected by micromobility, on-demand beam tracking can be a preferred option due to the similar mean attenuation and lower overhead involved in supporting continuous connectivity.

TABLE 8. Mean attenuation in dB for different applications and beam tracking settings.

beam tracking setting	Racing	Phone	VR	Video
On-demand	7.2224	2.5775	4.5634	2.4217
Regular, 20 ms	0.6240	2.3093	0.6361	2.4463
Regular, 80 ms	0.4862	2.3348	0.7321	2.4827
Regular, 160 ms	0.7486	2.3781	0.7754	2.4240
Regular, 320 ms	0.9719	2.3840	1.0402	2.4846
Regular, 1000 ms	5.1550	2.6219	8.7165	2.3211
Regular, 2000 ms	8.0280	3.4369	15.4802	2.3712

Utilizing the discussed statistical characteristics, specifics of individual experiments for blockage and micromobility, and the type of beam tracking considered, there are several important takeaways from the discussed behavior. First, unless the density of the blockers is extremely high, it is not a primary factor affecting the drop in the received signal strength below a given level, eventually resulting in decreased spectral efficiency. The micromobility resulting in degradation of the received signal strength was the most dominant factor between blockage events. The only feasible way to improve the behavior of the received signal strength is to increase the frequency of the beam-tracking time instants.

However, blockage occurs at much larger time scales even for high blocker densities in the environment.

When link distances are not large, such that blockage in the considered indoor environment may not always lead to outage events, and additional methods concealing its effects, such as 3GPP multiconnectivity option, may not be needed. As demonstrated in [9], the use of reflected paths at these short distances may provide reliable communications. However, this may change in different types of propagation environments characterized by larger propagation distances. As noted in [2], the mean received signal strength attenuation depends on the link distance and generally increases with it. Thus, the reported traces can only be utilized to analyze indoor deployments.

Finally, we would like to emphasize that in our study we considered the same heights for both Tx and Rx. In practical indoor deployments, the BS is expected to be mounted on a wall or ceiling at slightly higher heights. While this does not principally change the reported behavior of the traces as the principal point of body blockage is still either the head or chest, the impact of the blocker density is expected to be smaller as considered in the reported traces.

It is also worth noting that the equivalent isotropically radiated power (EIRP) is key parameter in designing a practical wireless system. The Tx and Rx used in the studies have an antenna gain of up to approximately 30 dB, making them potentially compliant with the EIRP of short-range systems in IMT-2030. This again demonstrates the importance of the obtained results for the further development of sub-THz wireless communications. Although this study primarily focuses on collecting data to enhance the sub-THz system analysis, our findings pave the way for the development of sub-THz systems with blockage avoidance and user mobility support.

VI. CONCLUSION

Motivated by the lack of received signal strength time series in sub-THz/THz bands under dynamic human body blockage and micromobility impairments, as well as different types of beam tracking procedures, we propose a trace generation procedure, as seen on the UE side. The procedure is based on realistic measurements of the blockage and measurement processes. The traces produced [11] can be further utilized for various tasks, including the assessment of the energy efficiency of sub-THz/THz communications and the development of statistical tests for discriminating blockage and micromobility events.

A. MAIN RESULTS

The analysis of the generated traces for different types of applications and beam-tracking procedures revealed that a maximum beam-tracking interval of 80 ms was sufficient to provide almost outage-free conditions for fast micromobility applications, whereas 320 ms was sufficient for slow micromobility applications. There are applications, such as video watching, for which even 320 ms is too short and



can be drastically increased to reduce the overhead. Out of all the considered applications, only the most dynamic ones, racing game, and VR, are characterized by significant differences between on-demand and regular beam tracking with 4-6.5 bits/Hz/s spectral efficiency degradation in the case of on-demand beam tracking compared to the regular one. For slow micromobility applications, no noticeable difference between the types of beam-tracking design was detected.

Finally, we highlight that the presence of micromobility impairments forces the reconsideration of various algorithms designed for mmWave and sub-THz systems. Blockage detection algorithms must be redesigned by accounting for the significant noise created by micromobility. Second, a new problem of determining the reason for an outage becomes important, as different actions need to be taken in the case of blockage and micromobility. Therefore, we created a library of traces that are available to the community.

We note that the methodology reported in this study is associated with several limitations and can therefore be enhanced in multiple ways. Specifically, in addition to focusing on a single frequency, 156 GHz, we also did not consider the impact of multiple blockers blocking the LoS path. Thus, a special question of interest is extending the traces to the case of multiple blockers simultaneously crossing the LoS path. As suggested by the recent studies [47], dynamics of signal attenuation in directive mmWave/sub-THz channels can be accurately predicted if blocking human is modeled as a dual-stage cylinder with two coaxial hexagons as bases of its top and bottom parts. Appearance of such an obstacle in the LoS path can result in a notable diffractive disruption with minimized back-scattering of the transmitted wavefront in small- and medium-sized premises. But the signal variations are relatively slow with the signal fall and recovery times equaling tens of milliseconds [2] for systems with Gaussian beams of a few degrees wide. In our studies, we employ antennas with a beamwidth of 8-10° compatible with the forecasts on the directivity of practical sub-THz wireless channels. It means that fast signal dynamics can be essentially determined by the human-induced beam misalignment between transmitting and receiving antennas in applications with moderate user activity. It is also worth noting that modern building materials, such as glass, whiteboard, concrete, exhibit 2-5 dB peak reflection losses [9]. But the contribution of undesirable secondary reflections to the increase in the signal to interference plus noise ratio is rather limited indoors since one way path loss can exceed 30 dB already at a link length of 3.5-4 m [9]. It has to be kept in mind, however, that for a far-field coverage in crowded areas the transmitted beam scatters off several obstacles. And the diffractive intensity distributions can further superimpose resulting in smoothing of the signal strength variations. Thus, a joint LoS blockage and micromobility scenario becomes a cornerstone in the assessment of the ultimate air interface properties for sub-THz systems. Due to the limitations of the modern sub-THz/THz equipment we emulated the process of bream searching. For the same reason, we had to perform blockage and micromobility measurements separately and then utilize the algorithm to join them together producing a joint time series. Finally, we also did not consider the case when the blockage itself might alter the optimal beam direction (e.g., by making a previously weaker non-LoS path temporarily more viable), thereby necessitating a beam searching procedure. This type of event may occur in practice. In our future work, we plan to relax some of these assumptions.

B. POTENTIAL APPLICATIONS AND FUTURE WORK

There are several critical functions of future 6G sub-THz/THz cellular systems that require the use of traces containing both micromobility and blockage jointly. One glaring example is to detect the reason for outage conditions when outages have already occurred. Specifically, dynamic human body blockage and UE micromobility are two impairments that may lead to loss of connectivity. However, the efficient handling of these events calls for fundamentally different actions from the system, with the former requiring a search for a BS, whereas the latter involves a beam-tracking procedure. Failure to differentiate the reason for an outage may lead to a prolonged time in outage conditions when blockage is misinterpreted as micromobility and/or a waste of system resources when micromobility is mistaken for blockage. The solution of this task requires an extension of the algorithms proposed so far for blockage-only conditions (see e.g. [3], [48]) that detect blockage events in noisy environments produced by micromobility.

It is also beneficial to distinguish between these micromobility and blockage events proactively such that there is sufficient time to preserve continuous service by utilizing, e.g., 3GPP multiconnectivity function. In principle, the same features can be utilized to distinguish outages caused by micromobility and blockage. However, instead of simple techniques utilized in, e.g. [3], [48], more comprehensive approaches are needed such as those capable of detecting specific patterns in noisy environments.

Of similar importance is the challenge of remote application detection using SRP statistics as it would allow to fine-tune the duration of the time between beam searching time instants. Similarly to blockage detection, both studies apply machine learning techniques to discriminate between "fast" and "slow" micromobility applications when micromobility is the only impairment in the SRP time series. In the presence of blockage, this might be problematic but still doable using more comprehensive ML-based approaches such as time-based convolutional neural networks (TB-CNN) or recurrent neural networks (TB-RNN) that could detect hidden patterns in limited data. Still these algorithms have to be learned using micromobility-only traces and then adapted to the noisy environment when blockage obscures (e.g., interrupts) micromobility-specific signatures.



Finally, the use of extremely large phased antenna arrays that are required to extend the coverage of prospective sub-THz/THz BS requires reconsidering the way beam searching is performed in systems with directional antennas. As compared to 5G NR, where the number of antenna configurations is limited to a few tens, sub-TH/THz systems require hundreds of configurations to be swept to restore the beam alignment. Accounting for the current configuration changing time that is on the order of a few microseconds and recalling that the slot duration in the future 6G sub-THz/THz system will likely be smaller than that of 5G NR to support ultra-reliable low latency service (URLLC), new advanced methods are required. By utilizing the reported traces with a sampling interval of just 50 μ s one may be designed and tested the proposed solutions in a close-to-reality environment.

REFERENCES

- 3GPP Commits to Develop 6G Specifications, 3GPP, Sophia Antipolis, France, May 2023.
- [2] A. Shurakov, D. Moltchanov, A. Prikhodko, A. Khakimov, E. Mokrov, V. Begishev, I. Belikov, Y. Koucheryavy, and G. Gol'tsman, "Empirical blockage characterization and detection in indoor sub-THz communications," *Comput. Commun.*, vol. 201, pp. 48–58, Mar. 2023.
- [3] F. Zhinuk, A. Gaydamaka, D. Moltchanov, and Y. Koucheryavy, "Spectral-based proactive blockage detection for sub-THz communications," *IEEE Commun. Lett.*, vol. 28, no. 7, pp. 1703–1707, Jul. 2024.
- [4] N. Stepanov, A. Turlikov, V. Begishev, Y. Koucheryavy, and D. Moltchanov, "Accuracy assessment of user micromobility models for THz cellular systems," in *Proc. 5th ACM Workshop Millim.-Wave Terahertz Netw. Sens. Syst.*, Oct. 2021, pp. 37–42.
- [5] N. Stepanov, D. Moltchanov, V. Begishev, A. Turlikov, and Y. Koucheryavy, "Statistical analysis and modeling of user micromobility for THz cellular communications," *IEEE Trans. Veh. Technol.*, vol. 71, no. 1, pp. 725–738, Jan. 2022.
- [6] D. Moltchanov, Y. Gaidamaka, D. Ostrikova, V. Beschastnyi, Y. Koucheryavy, and K. Samouylov, "Ergodic outage and capacity of terahertz systems under micromobility and blockage impairments," *IEEE Trans. Wireless Commun.*, vol. 21, no. 5, pp. 3024–3039, May 2022.
- [7] M. Giordani, M. Polese, A. Roy, D. Castor, and M. Zorzi, "A tutorial on beam management for 3GPP NR at mmWave frequencies," *IEEE Commun. Surveys Tuts.*, vol. 21, no. 1, pp. 173–196, 1st Quart., 2019.
- [8] V. Petrov, D. Moltchanov, Y. Koucheryavy, and J. M. Jornet, "Capacity and outage of terahertz communications with user micro-mobility and beam misalignment," *IEEE Trans. Veh. Technol.*, vol. 69, no. 6, pp. 6822–6827, Jun. 2020.
- [9] A. Shurakov, P. Rozhkova, A. Khakimov, E. Mokrov, A. Prikhodko, V. Begishev, Y. Koucheryavy, M. Komarov, and G. Gol'tsman, "Dynamic blockage in indoor reflection-aided sub-terahertz wireless communications," *IEEE Access*, vol. 11, pp. 134677–134689, 2023.
- [10] A. Ichkov, I. Gehring, P. Mähönen, and L. Simić, "Millimeter-wave beam misalignment effects of small- and large-scale user mobility based on urban measurements," in *Proc. 5th ACM Workshop Millimeter-Wave Terahertz Netw. Sens. Syst.*, Oct. 2021, pp. 13–18.
- [11] M. Ershova, A. Shurakov, Y. Koucheryavy, and G. Gol'tsman, "Synthetic received signal power data for 6G sub-terahertz cellular systems," *IEEE Dataport*, 2024. [Online]. Available: https://dx.doi.org/10.21227/f7qv-n928
- [12] F. Paonessa, G. Virone, S. Kianoush, A. Nordio, and S. Savazzi, "An initial study of human-scale blockage in sub-THz radio propagation with application to indoor passive localization," in *Proc. IEEE-APS Topical Conf. Antennas Propag. Wireless Commun. (APWC)*, Sep. 2024, pp. 50–54.
- [13] Y. Li, Y. Wang, Y. Lyu, Z. Yu, and C. Han, "220 GHz urban microcell channel measurement and characterization on a university campus," 2024, arXiv:2408.15772.

- [14] A. Shurakov, M. Ershova, A. Khakimov, A. Prikhodko, E. Mokrov, V. Begishev, G. Chulkova, Y. Koucheryavy, and G. Gol'tsman, "Remote detection of applications for improved beam tracking in mmWave/sub-THz 5G/6G systems," 2024, arXiv:2410.18637.
- [15] T. Doeker, L. H. Loeser, and T. Kürner, "Measurements and verification of an antenna pattern-based tracking algorithm at 300 GHz," *IEEE Trans. Terahertz Sci. Technol.*, vol. 15, no. 3, pp. 359–369, May 2025.
- [16] J. Lee, J.-J. Park, K.-W. Kim, H. K. Kwon, and M.-D. Kim, "Measurement-based omnidirectional millimetre-wave and sub-THz propagation analysis in a large cubicle office environment," *IET Microw., Antennas Propag.*, vol. 17, no. 6, pp. 443–453, May 2023.
- [17] J. Lee, J.-J. Park, K.-W. Kim, H. K. Kwon, and M.-D. Kim, "Sub-THz outdoor urban measurements and multipath propagation characteristics," in *Proc. 17th Eur. Conf. Antennas Propag. (EuCAP)*, Mar. 2023, pp. 1–4.
- [18] S. Ju and T. S. Rappaport, "142 GHz multipath propagation measurements and path loss channel modeling in factory buildings," in *Proc. IEEE Int. Conf. Commun.*, May 2023, pp. 5048–5053.
- [19] J.-J. Park, J. Lee, J. Liang, K.-W. Kim, K.-C. Lee, and M.-D. Kim, "Millimeter wave vehicular blockage characteristics based on 28 GHz measurements," in *Proc. IEEE 86th Veh. Technol. Conf. (VTC-Fall)*, Sep. 2017, pp. 1–5.
- [20] V. Begishev, E. Sopin, D. Moltchanov, R. Kovalchukov, A. Samuylov, S. Andreev, Y. Koucheryavy, and K. Samouylov, "Joint use of guard capacity and multiconnectivity for improved session continuity in millimeter-wave 5G NR systems," *IEEE Trans. Veh. Technol.*, vol. 70, no. 3, pp. 2657–2672, Mar. 2021.
- [21] V. Begishev, E. Sopin, D. Moltchanov, R. Pirmagomedov, A. Samuylov, S. Andreev, Y. Koucheryavy, and K. Samouylov, "Performance analysis of multi-band microwave and millimeter-wave operation in 5G NR systems," *IEEE Trans. Wireless Commun.*, vol. 20, no. 6, pp. 3475–3490, Jun. 2021.
- [22] E. Sopin, D. Moltchanov, A. Daraseliya, Y. Koucheryavy, and Y. Gaidamaka, "User association and multi-connectivity strategies in joint terahertz and millimeter wave 6G systems," *IEEE Trans. Veh. Technol.*, vol. 71, no. 12, pp. 12765–12781, Dec. 2022.
- [23] H. Zhang, N. Shlezinger, F. Guidi, D. Dardari, M. F. Imani, and Y. C. Eldar, "Beam focusing for near-field multiuser MIMO communications," *IEEE Trans. Wireless Commun.*, vol. 21, no. 9, pp. 7476–7490, Sep. 2022.
- [24] J. Durnin, J. H. Eberly, and J. J. Miceli, "Comparison of Bessel and Gaussian beams," *Opt. Lett.*, vol. 13, no. 2, pp. 79–80, 1988.
- [25] Y. Xing and T. S. Rappaport, "Propagation measurement system and approach at 140 GHz-moving to 6G and above 100 GHz," in *Proc. IEEE Global Commun. Conf.*, Dec. 2018, pp. 1–6.
- [26] J. M. Eckhardt, V. Petrov, D. Moltchanov, Y. Koucheryavy, and T. Kurner, "Channel measurements and modeling for low-terahertz band vehicular communications," *IEEE J. Sel. Areas Commun.*, vol. 39, no. 6, pp. 1590–1603, Jun. 2021.
- [27] V. Petrov, J. M. Eckhardt, D. Moltchanov, Y. Koucheryavy, and T. Kurner, "Measurements of reflection and penetration losses in low terahertz band vehicular communications," in *Proc. 14th Eur. Conf. Antennas Propag.* (EuCAP), Mar. 2020, pp. 1–5.
- [28] K. Du, O. Ozdemir, F. Erden, and I. Guvenc, "Sub-terahertz and mmWave penetration loss measurements for indoor environments," in *Proc. IEEE Int. Conf. Commun. Workshops (ICC Workshops)*, Jun. 2021, pp. 1–6.
- [29] Y. Wu, J. Kokkoniemi, C. Han, and M. Juntti, "Interference and coverage analysis for terahertz networks with indoor blockage effects and line-ofsight access point association," *IEEE Trans. Wireless Commun.*, vol. 20, no. 3, pp. 1472–1486, Mar. 2021.
- [30] V. Petrov, D. Moltchanov, Y. Koucheryavy, and J. M. Jornet, "The effect of small-scale mobility on terahertz band communications," in *Proc. 5th* ACM Int. Conf. Nanosc. Comput. Commun., Sep. 2018, pp. 1–2.
- [31] S. Dugaeva, V. Begishev, E. Mokrov, and K. Samouylov, "Using motion sensors for improved beam tracking in THz communications with user micromobility," in *Proc. Int. Conf. Modern Netw. Technol. (MoNeTec)*, Oct. 2022, pp. 1–8.
- [32] S. Dugaeva, V. Begishev, and N. Stepanov, "Utilization of machine learning algorithms to identify user applications," in *Proc. Int. Conf. Distrib. Comput. Commun. Netw.*, 2024, pp. 410–422.
- [33] NR; Physical Channels and Modulation, document TS 38.211, 3GPP, Dec. 2017.
- [34] NR; Medium Access Control (MAC) Protocol Specification, document TR 38.321, 3GPP, Jul. 2022.
- [35] NR; Physical Layer Procedures for Control, document TR 38.213, 3GPP, Jun. 2022.



- [36] S. Nagaraja and T. Luo, "Beam selection and radio link failure during beam recovery," U.S. Patent 15 707 626, Jul. 19, 2018.
- [37] Technical Feasibility of IMT in Bands Above 100 GHz, document ITU-R M.2541-0, May 2024.
- [38] Y. Banday, G. Mohammad Rather, and G. R. Begh, "Effect of atmospheric absorption on millimetre wave frequencies for 5G cellular networks," *IET Commun.*, vol. 13, no. 3, pp. 265–270, Feb. 2019.
- [39] NR; Multi-connectivity; Stage 2, document TS 37.340, 3GPP, Dec. 2019.
- [40] E. Khayrov and Y. Koucheryavy, "Packet level performance of 5G NR system under blockage and micromobility impairments," *IEEE Access*, vol. 11, pp. 90383–90395, 2023.
- [41] D. Moltchanov, V. Beschastnyi, D. Ostrikova, Y. Gaidamaka, and Y. Koucheryavy, "Uninterrupted connectivity time in THz systems under user micromobility and blockage," in *Proc. IEEE Global Commun. Conf.* (GLOBECOM), Dec. 2021, pp. 01–06.
- [42] A. Ali, O. Galinina, J. Hosek, and S. Andreev, "Effects of micro-scale mobility and beam misalignment in on-body mmWave systems," *IEEE Commun. Lett.*, vol. 28, no. 3, pp. 682–686, Mar. 2024.
- [43] D. Moltchanov, A. Ometov, and Y. Koucheryavy, "Analytical characterization of the blockage process in 3GPP new radio systems with trilateral mobility and multi-connectivity," *Comput. Commun.*, vol. 146, pp. 110–120, Oct. 2019.
- [44] R. Kovalchukov, D. Moltchanov, Y. Gaidamaka, and E. Bobrikova, "An accurate approximation of resource request distributions in millimeter wave 3GPP new radio systems," in *Proc. Int. Conf. Next Gener. Wired/Wireless Netw.* Cham, Switzerland: Springer, 2019, pp. 572–585.
- [45] G. Charan, M. Alrabeiah, and A. Alkhateeb, "Vision-aided dynamic blockage prediction for 6G wireless communication networks," in *Proc. IEEE Int. Conf. Commun. Workshops (ICC Workshops)*, Jun. 2021, pp. 1–6.
- [46] M. Alrabeiah and A. Alkhateeb, "Deep learning for mmWave beam and blockage prediction using sub-6 GHz channels," *IEEE Trans. Commun.*, vol. 68, no. 9, pp. 5504–5518, Sep. 2020.
- [47] S. Mukherjee, G. Skidmore, T. Chawla, A. Bhardwaj, C. Gentile, and J. Senic, "Scalable modeling of human blockage at millimeter-wave: A comparative analysis of knife-edge diffraction, the uniform theory of diffraction, and physical optics against 60 GHz channel measurements," *IEEE Access*, vol. 10, pp. 133643–133654, 2022.
- [48] S. Wu, M. Alrabeiah, A. Hredzak, C. Chakrabarti, and A. Alkhateeb, "Deep learning for moving blockage prediction using real mmWave measurements," in *Proc. IEEE Int. Conf. Commun.*, May 2022, pp. 3753–3758.



VITALII BESCHASTNYI received the B.Sc. and M.Sc. degrees in applied mathematics and informatics from the Peoples' Friendship University of Russia (RUDN University), in 2014 and 2016, respectively, and the Ph.D. degree in applied mathematics and computer science, in 2020. He is the author of more than 50 scientific and conference papers on resource allocation in 5G networks, applied queuing and teletraffic theory, and system-level simulation of heterogeneous

networks. His research interests include the study of 5G/5G+ wireless communication networks, analysis of the quality of service, performance evaluation, and simulation of wireless networks with enabled V2X communications, and THz band communications.



MARGARITA ERSHOVA received the B.S. degree in fundamental physics from Moscow Pedagogical State University, Moscow, Russia, in 2024. She is currently pursuing the M.S. degree in applied electronics and photonics from the HSE Tikhonov Moscow Institute of Electronics and Mathematics, HSE University, Moscow.

She is a Junior Research Assistant with the Laboratory of Quantum Detectors, Moscow Pedagogical State University. Her scientific research

interests include sub-terahertz metrology, design and prototyping of microwave electronic and photonic circuits, and sub-terahertz 5/6G wireless communications.



DARYA OSTRIKOVA received the B.Sc. and M.Sc. degrees in applied mathematics from the Peoples' Friendship University of Russia (RUDN University), in 2010 and 2012, respectively, and the Ph.D. degree in applied mathematics and computer science, in 2015. Since 2012, she has been with the Telecommunication Systems Department, RUDN University, where she is currently an Associate Professor with the Department of Applied Probability and Informatics. She is the author of

more than 50 scientific and conference papers on analytical performance analysis of various 5G/5G+ technologies, applied queuing and teletraffic theory, and system-level simulation of heterogeneous networks. Her current research interest includes the performance analysis of 5G/5G+ wireless networks



VLADISLAV PROSVIROV received the B.Sc. degree in applied mathematics and informatics and the M.Sc. degree in fundamental informatics and information technologies from RUDN University, Moscow, Russia, in 2019 and 2021, respectively. Currently, he is pursuing the Ph.D. degree in electronics, radio engineering, and communication systems with the Higher School of Economics, HSE University. His research interests include 5G/5G+ network performance analysis.

UAV-based scenarios in mmWave networks, channel modeling, and artificial intelligence.



ALEXANDER SHURAKOV received the Specialist degree in physics and computer science from the Vyatka State University of Humanities, Russia, and the Ph.D. degree in radiophysics from the Kotelnikov Institute of Radioengineering and Electronics, Russian Academy of Sciences, in 2019

In 2008, he joined the Radiophysics Laboratory, Moscow Pedagogical State University, Moscow, Russia, as a Graduate Student. In 2010, he qual-

ified for a Fellowship Program with the Harvard-Smithsonian Center for Astrophysics, where he continued to work on cryogenic heterodyne receivers for radio astronomy, until 2013. He is currently an Associate Professor with the Department of General and Experimental Physics, Moscow Pedagogical State University, and a Senior Researcher with the Department of Quantum Optics and Telecommunications, HSE University, Moscow. He has coauthored dozens of scientific articles on super- and semiconductor electronic and radio-photonic circuits for terahertz remote sensing and sub-terahertz wireless communications. He has been a principal investigator and key implementer of numerous scientific projects in the aforementioned research areas. In 2021, he was awarded a stipend from the Ministry of Industry and Trade of the Russian Federation for his significant contribution to the development of terahertz devices and systems.





YULIYA GAIDAMAKA received the Ph.D. and the Full Doctor of Science degrees in mathematics from the Peoples' Friendship University of Russia (RUDN University), in 2001 and 2017, respectively. Since 2001, she has been an Associate Professor. She is currently a Professor with the Applied Probability and Informatics Department, University. She is the author of more than 200 scientific and conference papers, and the co-author of three monographs on multiplicative solutions

of finite Markov chains, matrix, and analytical methods for performance analysis of wireless heterogeneous networks. Her current research focuses on performance analysis of 5G+ networks, queuing theory, and mathematical modeling of communication networks, including admission control and radio resource management using artificial intelligence.



YEVGENI KOUCHERYAVY received the Ph.D. degree from the Tampere University of Technology (TUT), Finland. He is the author of numerous publications in the field of advanced wired and wireless networking and communications. His current research interests include various aspects of heterogeneous wireless communication networks and systems.



GREGORY GOL'TSMAN received the Ph.D. degree in physics of semiconductors from Moscow Pedagogical State University, Moscow, Russia, in 1973. He is currently a Professor and the Chair of the Department of General and Experimental Physics, Moscow Pedagogical State University, and the Department of Quantum Optics and Telecommunication, HSE University, Moscow. He is a Pioneering Physicist. His past achievements include: the first observation of optical

transitions between energy levels of excitons in monocrystalline semiconductors, the discovery of the negatively charged state of shallow donors and the positively charged state of shallow acceptors in monocrystalline semiconductors, the study of electronic energy relaxation in disordered films of superconductors, the discovery and promotion of the superconducting hot electron bolometric mixer, and the superconducting single-photon detector. He has won several prizes, including the stipend from the Soros Foundation for Professors, from 1996 to 2001, the IEEE Van Duzer Prize in Applied Superconductivity, in 2010, and the IEEE Award for Continuing and Significant Contributions in the Field of Applied Superconductivity, in 2017. In 2005, he founded a start-up company called Scontel, which produces ready-to-use superconducting receivers for near and far-infrared wavelengths. In 2015, an innovative company named TIRPhotonics LLC was established within the Skolkovo Foundation. This company develops and manufactures optical integrated chips (including quantum chips) for modern scientific experiments and instruments.

. . .